Biosensors and Bioelectronics 130 (2019) 414–419

Contents lists available at ScienceDirect

Biosensors and Bioelectronics

journal homepage: www.elsevier.com/locate/bios

Highly sensitive and accurate estimation of bloodstain age using smartphone

Wooseok Choi[a,1], Joonchul Shin[a,1], Kyung-A Hyun[a], Jaewoo Song[b], Hyo-Il Jung[a,*]

[a] School of Mechanical Engineering, Yonsei University, Seoul, Republic of Korea
[b] Department of Laboratory Medicine, Yonsei University College of Medicine, Severance Children's Hospital, Seoul, Republic of Korea

ARTICLE INFO

Keywords:
Bloodstain age
Pattern recognition
Blood pool
Crack ratio
Brightness value
Smartphone

ABSTRACT

The estimation of bloodstain age is an important factor in forensic analysis. Previously, we have reported a smartphone-based colorimetric system for age estimation of bloodstain, in which Whole blood and EDTA whole blood were dropped on 4 different materials (700 μL) and captured using a smartphone for 72 h. In order to enhance sensitivity and accuracy of the previous system, the current work is dedicated towards the application of pattern recognition and classification of bloodstain images based on a smartphone. Three detection methods (blood pool, crack ratio, and colorimetric analysis) in terms of 6 steps of drying process of the bloodstain (coagulation, gelation, edge desiccation, center desiccation, crack propagation, and final desiccation) were applied to estimate age of the bloodstain accurately. Three parameters from the bloodstain images were then classified as comparing to those of stored reference images with similar trends in database. The bloodstain age was successfully determined by 9 h, 18 h, and 48 h with respect to the three detection methods mentioned above, respectively. The differences in bloodstain images were clearly distinguished every hour by using smartphone-based pattern recognition analysis. Therefore, our system is expected to shed a light on the field of forensic science by estimating bloodstain age in real time.

1. Introduction

Bloodstain, the traces left on the crime scene, is one of the key factors for elucidation of history of crime scene, thus playing a major role in forensic science (James et al., 2005; Bremmer et al., 2012). The RNA analysis and reflection spectroscopy were conventionally introduced in order to track genetic information and age estimation of bloodstains, respectively. In the stated method, RNA from the blood was extracted for determination of the degree of degradation of the RNA over time (Bauer et al., 2003). The reflection spectroscopy was applied to analyze the oxidation of hemoglobin in response to time (Bremmer et al., 2011). The reflectance values of each oxy-hemoglobin (HbO_2), met-hemoglobin (met-Hb) and hemichrome (HC) fraction were determined in terms of wavelengths by the spectroscopy. However, these measurements require exorbitant cost and consume time to estimate the bloodstain age, thereby rarely applying them to the spot. To address these issues, we have recently reported smartphone-based colorimetric analysis system without using any additional equipment for age estimation of bloodstains using color change caused by oxidation of blood because a high-level image sensor for colorimetric analysis application is built in a smartphone (Shin et al., 2017). The bloodstains exposed to air was observed in physicochemical changes, such as color variation and change in the form of blood. The oxidation of bloodstain resulted in transformation of hemoglobin into HbO_2, met-Hb, and HC, thereby changing color from bright red to dark red. After the incident, early response is required to trace the crime, so it was important to improve accuracy in the early time zone. However, the low color resolution was observed in the early time zone (0–9 h) in our previous report although age estimation of the bloodstain was successfully done by 48 h. In this study, a more accurate smartphone-based pattern recognition was designed for enhancing accuracy in the early time zone compared with our previous work. The blood exposed to air caused a formation of fibrin in a net structure to cause coagulation of blood, gelation and crack formation, consecutively during drying process (Brutin et al., 2011; Sobac and Brutin, 2014; Laan et al., 2016). The area of the liquid state that remains during the drying process is blood pool, and it decreases as the water evaporates over time. The rate of pixels observed in the blood pool, crack ratio and the colorimetric analysis method for inner circle area of bloodstains were calculated over time using three characteristics of blood. The area ratio of the blood pool, crack ratio over the bloodstain, and color intensities of the captured bloodstains were compared with those of reference images in order to classify images that had similar trends. Thus, we were successfully able to enhance the sensitivity and accuracy of our previous

* Corresponding author.
E-mail address: uridle7@yonsei.ac.kr (H.-I. Jung).
[1] The authors contributed equally to this work.

https://doi.org/10.1016/j.bios.2018.09.017
Received 30 June 2018; Received in revised form 27 August 2018; Accepted 4 September 2018
Available online 05 September 2018
0956-5663/

method in terms of applying blood pool analysis, crack ratio analysis, and colorimetric analysis to the bloodstain.

2. Materials and methods

2.1. Preparation of materials and blood samples

The blood samples (700 μL) were dropped on glass, wood, paper, and fabric (10 × 10 cm) in order to analyze the bloodstain age in the various experimental conditions. In addition, we chose these four materials, which represent parameters that can be found anywhere, whether at home or in the office. In order to apply three detection methods (blood pool analysis, crack ratio analysis, and colorimetric analysis) to the age estimation of the bloodstain, we captured the bloodstain images by using a smartphone (Samsung Galaxy note 3) for 72 h. The bloodstain images were consecutively captured every hour until 9 h passed (blood pool analysis), where the blood was completely dried, whereas they were recorded every 6 h for 3 days (crack ratio analysis and colorimetric analysis) after 9 h under the following condition: 30% humidity. Three healthy participants (average age of 29.75 and average hemoglobin concentration of 15.5 g/dL) and three participants (average age of 32.35) with different concentration of hemoglobin donated blood (10 mL) to our team, respectively. In addition, the hemoglobin concentration in each sample was offered by Severance Children's Hospital where a CBC (Complete Blood Count) analyzer was applied to measure the subjects' hemoglobin concentration. This study was conducted in accordance to the guidelines of human research established by the Institutional Review Board (IRB) of Severance Children's Hospital, Yonsei University.

2.2. Principle of drying process and deformation in bloodstain

The drying process of bloodstains consists of the following 6 steps: coagulation, gelation, edge desiccation, center desiccation, crack propagation, and final desiccation (Fig. 1). The platelets in the exposed air were destroyed, changing the shape of the blood during the formation of thromboplastin. Thromboplastin consecutively conjugated with calcium ions in the blood, transformed prothrombin into thrombin. The fibrinogen then became a thread-like substance called fibrin after reacting with thrombin (Furie and Furie, 1988; Gaertner and Massberg, 2016). The area of the blood pool, the area of the liquid state, was gradually reduced in response to beginning of drying process, where the bloodstains were exposed to air. The particles in the center of the bloodstains migrated to the surface, accumulating at the boundary of the blood pool as known as coffee ring effect (Deegan et al., 1997; Kuo et al., 2011; Chen et al., 2018) and transforming into gel form as the surface of the bloodstain dried, thereby increasing the area of desiccated bloodstain (Dugyala et al., 2016).

The crack began to form due to the repulsive force of the bloodstain-substrate and bloodstain-atmosphere (Sobac and Brutin, 2014). The contact force between the bloodstain and substrate maintained the initial shape during the drying process of bloodstains whereas the area of blood pool was shrunk due to H_2O evaporation from the interface of bloodstain and air. The conflict between contact force and shrinkage force from H_2O removal resulted in tensile stress on the bloodstains, which triggered structural change in the bloodstain (Lei et al., 2002).

In addition, a transformation and oxidation of oxy-hemoglobin due to O_2 saturation brought about the formation of methemoglobin and the color variation of the bloodstains from bright red to dark red (Bremmer et al., 2011) at the beginning of the drying process. Methemoglobin turned into hemichrome, which decreased brightness value of the bloodstains.

2.3. Detection methods and algorithms for prediction of bloodstain age

These types of detection methods are primarily employed for enhancement of sensitivity and accuracy of detection system for age estimation of bloodstains, namely blood pool analysis, crack ratio analysis, and colorimetric analysis. These methods are applied on different stages of the smartphone-based pattern recognition system – coagulation, gelation, edge desiccation, center desiccation, crack propagation, and final desiccation as shown in Fig. 1, respectively. The methods in Fig. 2 can be briefly explained as follows – in the first detection method (blood pool analysis), scanning from 0 to 100 pixels in units of 10 (a section) was done to find a starting point where color intensities changed rapidly. The slope of each section during pixel scanning was then compared by increments of consecutive 10 units. Our system then automatically detected color intensities of the pixel at a point (Red value ≥ 200) where the slope suddenly changed in each direction and displayed a circle with points. The measurement system after detection of outer circle of the bloodstain scanned the inner part of the bloodstain in the same way, capturing each point where the color intensity rapidly decreased (Red value ≥ 200) and drawing the inner circle likewise as finding the outer circle of the bloodstain as shown in Fig. 2(a). In the light of the above, the change in ratio of the inner and outer circle was then calculated over time to estimate the age of the bloodstain in the following Eq. (1), where the $f(x)$ denotes a boundary of outer circle, A refers to total area of the bloodstain, and Δx stands for the differential of the variable x.

$$\int f(x)dx/\mathrm{A} = \lim_{n\to\infty} \sum_{i=1}^{n} f(x_i^*)\Delta x/\mathrm{A} \tag{1}$$

The number of white pixels over total area of the bloodstain, crack ratio, was considered as the second detection method for estimation of bloodstain age (0 – 18 h) after blood pool analysis. The smartphone-based pattern recognition system automatically converted RGB (Red, Green, and Blue) values of the captured image into binary scale image, thereby counting a number of all the white pixels from the image. Once the system converted a bloodstain image from RGB to binary scale, the white pixels of the image were identified by blue boundary lines as shown in Fig. 2(b). In addition, the ratio of white pixels was determined by dividing the number of pixels in the entire bloodstain image after counting the number of all white pixels in the bloodstain. Finally, the third method, colorimetric analysis, was applied to the system in order to estimate the overall bloodstain age from 0 to 48 h. The variation of the brightness (V) values in the bloodstain was observed every hour by using the RGB values of the pixels in the white box. The color intensities of all the pixels above each line were consecutively scanned and stored n times as shown in Fig. 2(c). The measurement system divided the color values of all the pixels by the number of counted pixels to obtain each R, G, and B value. In addition, since the sensitivity of the V values was the highest of these parameters, the V values of HSV (Hue, Saturation, and Brightness) were then calculated from the collected RGB using the following set of Eqs. (2)–(4) (Yang et al., 2017; Yu et al., 2015; Lee et al., 2014; Yamanaka et al., 2018). Moreover, we have designed the detection algorithm for three different stages: initial stage, analysis stage, and final stage in Fig. 2. In the initial stage, the system scanned the bloodstain image after material selection that the bloodstains were dropped. The novel three detection methods were automatically applied to the captured images, thereby comparing blood pool ratio, crack ratio, and color intensities of the captured bloodstains with those of reference images, which were already stored in the database. Finally, the smartphone-based pattern recognition system displayed the estimated time for the bloodstains and saved data from the classified images to the database. The operation of our system is demonstrated in Fig. S1.

$$H = \cos^{-1}\frac{\frac{1}{2}[(R-G)+(R-B)]}{\sqrt{(R-G)^2+(R-B)(G-B)}} \tag{2}$$

$$S = 1 - \frac{3}{(R+G+B)}[MIN(R,G,B)] \tag{3}$$

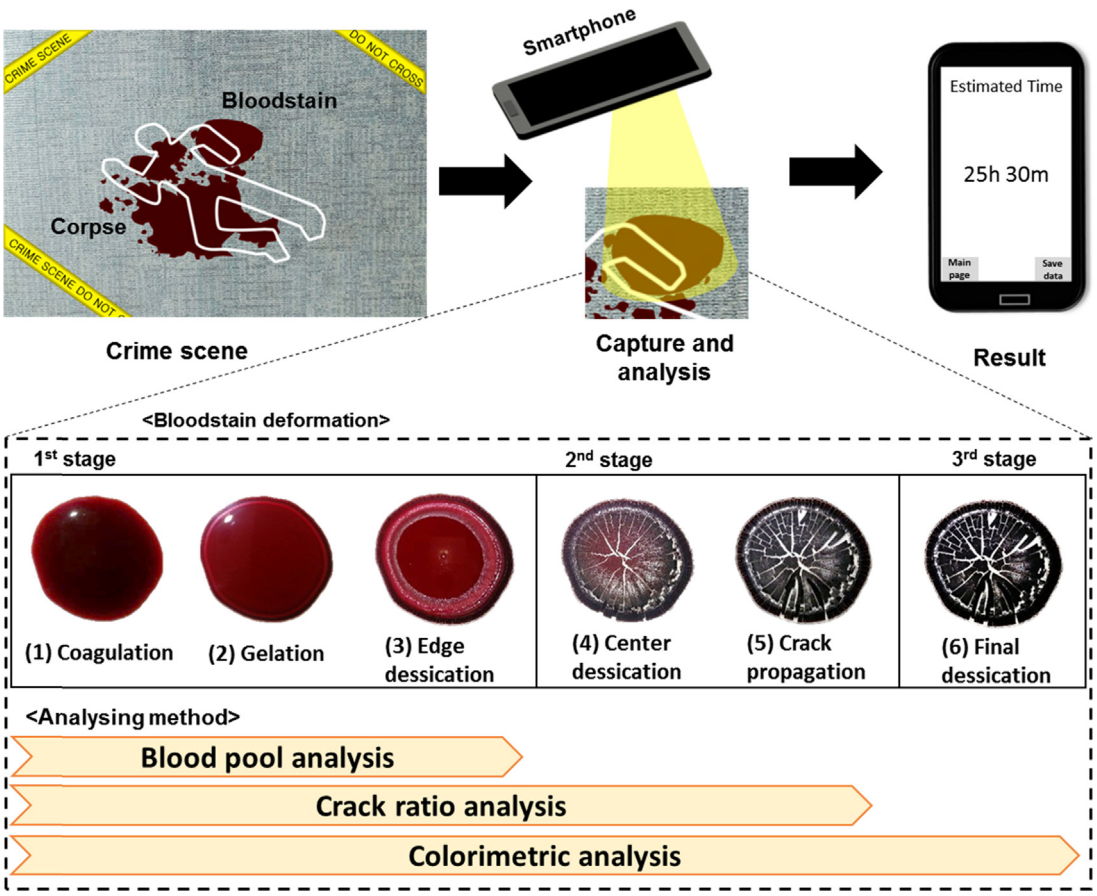

Fig. 1. Schematic diagrams of the estimation system for bloodstain age. Detection methods for estimating bloodstain age include three consecutive stages: blood pool analysis, crack ratio analysis and colorimetric analysis. These methods are applied on different stages of the smartphone-based pattern recognition system – coagulation, gelation, edge desiccation, center desiccation, crack propagation, and final desiccation.

$$V = Max(R, G, B) \quad (4)$$

3. Results and discussion

3.1. Effects of different types of materials on bloodstain characteristics

The images of EDTA whole blood (700 μL) dropped on 4 different materials (glass, wood, paper, and fabric) were captured by our system as shown in Fig. 3(a) and Fig. S2. In order to estimate age of the bloodstains accurately, we divided the analytical methods for drying process of bloodstains into 3 stages: blood pool analysis, crack ratio analysis, and colorimetric analysis. The blood pool ratio over total area of the bloodstain gradually decreased, thereby completely drying the bloodstain within 9 h in the first stage (Fig. 3(b)); the CV (Coefficient of Variation) of the blood pool ratio in 4 different materials was calculated as 0.0%, 0.3%, 0.1%, 0.1%, 0.5%, 2.4%, 2.3%, 0.0%, 0.0% and 0.0% on glass, 0.0%, 0.6%, 0.5%, 1.9%, 2.5%, 2.8%, 5.9%, 0.4%, 0.0% and 0.0% on wood and 0.0%, 1.2%, 1.6%, 0.2%, 1.8%, 0.4%, 1.4%, 0.8%, 2.7%, and 6.5% on paper and 0.0% on fabric over time, respectively (Table S1).

In addition, the white pixels of the bloodstain increased by gradual crack formation, enabling to count the variation of the white pixels over the bloodstain until 18 h passed in Fig. 3(c), whereas the V values of the bloodstain gradually decreased by 48 h as shown in Fig. 3(d). The CV (Coefficient of Variation) of the crack ratio in 4 different materials was calculated as 0.0%, 3.4%, 2.3%, 1.6%, 3.3%, 4.4%, 4.7%, 3.2%, 3.2%, 2.1%, 2.8%, 2.7% and 2.6% on glass, 0.0%, 6.3%, 4.0%, 5.7%, 3.3%, 3.3%, 3.8%, 9.4%, 8.2%, 5.9%, 7.8%, 6.0% and 4.1% on wood and 0.0%, 4.9%, 3.8%, 3.8%, 5.0%, 5.6%, 5.2%, 5.7%, 4.7%, 4.8%, 5.1%, 6.0%, and 4.5% on paper and 0.0% on fabric in terms of time, respectively (Table S1). The spread of blood on the materials in the order of paper, wood, glass, and fabric caused rapid evaporation of the bloodstain, thereby resulting in a sharp decrease of the blood pool ratio over total area of the bloodstain. Moreover, the ratio of crack formation to the bloodstain varied in response to the degree of moisture absorption of each material; the less H_2O absorption for a degree of porosity of the materials, especially in glass (no porosity), brought about large amount of crack formation from the bloodstain. Finally, the highest V values were detected on the material where the bloodstain was widely spread, transmitting light source fully due to minimum concentration of hemoglobin per unit area.

On the other hand, the colorimetric analysis method was only applied to the bloodstain on a fabric material since blood was completely absorbed, preventing the formation of blood pool and cracks; the CV (Coefficient of Variation) of the V values in 4 different materials was calculated as 4.6%, 1.4%, 1.4%, 5.7%, 1.7%, 3.6%, 3.8%, 2.0%, 2.0%, 1.5%, 1.0%, 4.0% and 4.5% on glass, 2.0%, 3.7%, 4.7%, 1.7%, 4.8%, 6.5%, 4.1%, 1.0%, 2.1%, 2.1%, 4.2%, 3.2%, and 2.1% on wood, 5.0%, 4.0%, 1.8%, 4.4%, 2.7%, 3.3%, 3.3%, 1.7%, 1.7%, 0.9%, 1.7%, 1.7% and 1.3% on paper and 4.6%, 4.0%, 6.1%, 5.0%, 2.9%, 1.0%, 2.8%, 1.4%, 1.4%, 0.9%, 2.0%, 1.5%, and 1.5% on fabric in response to time, respectively (Table S1). The bloodstain age was able to be accurately calculated by using the following equations from the drying process of the bloodstain on each material where the blood was dropped via the smartphone-based pattern recognition system. Furthermore, whole blood samples were dried an hour faster than EDTA whole blood, whereas no significant difference among blood pool ratio, white pixel ratio (crack) over total area of the bloodstain, and trend lines toward

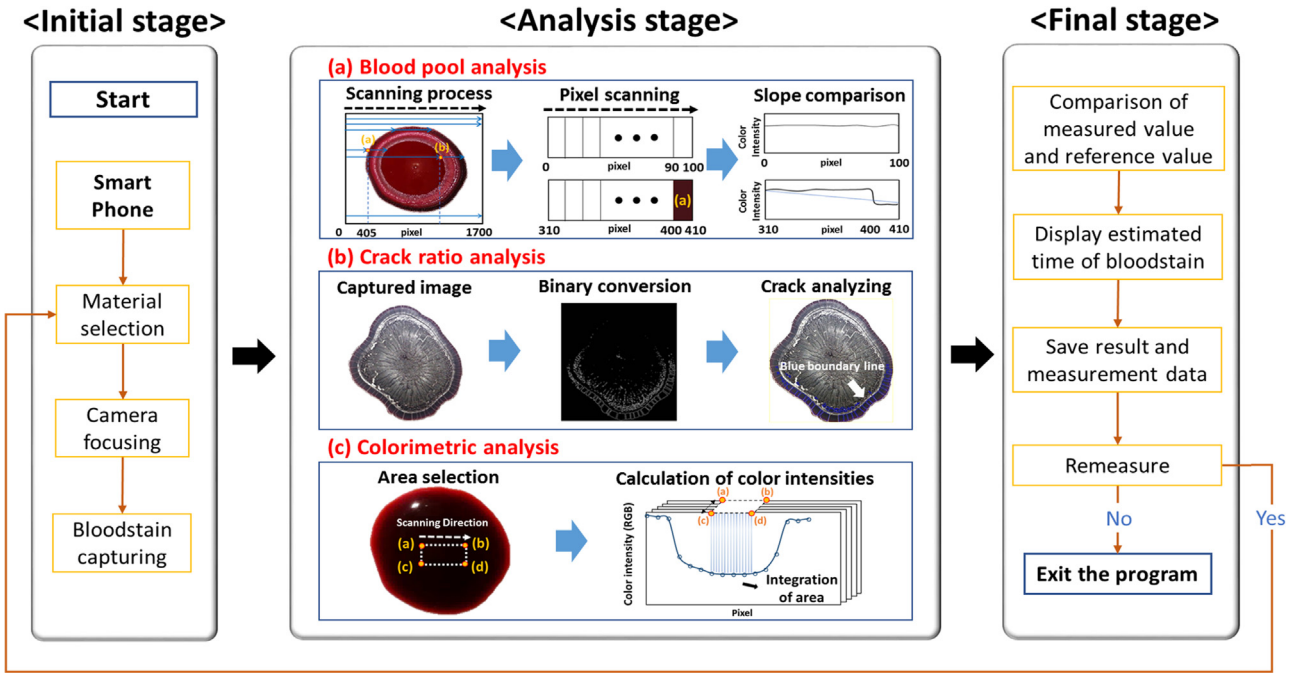

Fig. 2. The flowchart (Initial stage, Analysis stage, and Final stage) and the three different detection methods for estimation of bloodstain age: Blood pool analysis, Crack ratio analysis, and Colorimetric analysis. The flowchart contains comparison between reference data and measured data to enhance accuracy of the measurement of bloodstains. (a) The ratio of blood pool area over the total area of the bloodstain was calculated from scanning red color pixels. (b) The cracks of the bloodstains were detected by binary scale conversion of the image, thereby counting white pixels of the crack. (c) The color intensities of the bloodstain were measured the variation of color intensities over time. (For interpretation of the references to color in this figure legend, the reader is referred to the web version of this article.).

variation of V values was observed as shown in Fig. S3 ($p < 0.05$). The LOD (Limit of Detection) of our system was 0.1%, 15%, and 7.6% for blood pool, crack ratio, and V values, respectively.

According to the slopes of crack ratio and the level of moisture absorption for each material, the rate of crack formation against the bloodstains were determined by the following Eq. (5), where the *Mi* denotes an increase rate for weight of each material, *Ma* refers to mass of materials absorbed by the blood, and *Mo* and *Vw* stand for original weight of each material and the blood, respectively. The rate of moisture absorption on each material increased in the following order: glass (0.0%), paper (11.4%), wood (48.6%), and fabric (100%). H_2O absorption of the bloodstain on each material resulted in less surface tension between the blood and the material. Thus, we were able to observe more cracks (white pixels) of the bloodstain on the glass, rarely absorbing H_2O from the blood, were formed than those on 3 different materials as shown in Table 1.

$$M_i(\%) = \frac{(M_a - M_o)}{V_w} \times 100 \quad (5)$$

3.2. Analysis of the three parameters of the bloodstain relative to temperature and hemoglobin concentration

The bloodstains, dropped on glass at 4 different temperature (-15, 5, 23, and 36 °C) and hemoglobin concentration (8.7, 10.3, 15.5, and 17.3 g/dL), were measured over time by using 3 types of detection methods due to changing the pattern of bloodstain formation in response to temperature, concentration of hemoglobin, and drying process time (Fig. S4 and S5). The blood was not absorbed into glass against other 3 materials, thereby conserving the physical properties of the bloodstain, such as reduction rate of blood pool area, crack formation ratio, and decrease in the V values, so that we dropped the blood on glass. As shown in Fig. 4(a)-(c), the blood pool was completely dried within 4–9 h and white pixel ratio over total area of the bloodstain increased by 18–30 h, whereas V values continuously decreased until 48 h passed in 4 different temperature. The blood pool was rapidly disappeared from the bloodstain at high temperature since temperature increase triggered to accelerate evaporation rate of H_2O in the bloodstain (Hu and Larson, 2002). Furthermore, high temperature stimulated vaporization between bloodstain and atmosphere, thereby increasing gradually force difference between bloodstain-substrate and bloodstain-atmosphere and forming drastically a number of white pixels from the bloodstain. The binding of hemoglobin and oxygen formed HbO_2, increasing brightness of the bloodstain temporarily. On the other hand, oxidation of HbO_2 transformed HbO_2 into met-Hb and HC, decreasing the V values of the bloodstain sharply. In other words, the oxidation rate was dependent on temperature change.

In addition, a number of hemoglobin per unit area caused the reduction of blood pool area, the formation of cracks from the bloodstain, and the variation of the V values in Fig. 5(a)-(c). The contents of H_2O in the same blood volume is different in response to hemoglobin concentrations (Hu et al., 2012) since H_2O ratio is dependent on an amount of red blood cells; the higher hemoglobin concentration causes the less time spent for drying of the blood and decreases blood pool ratio rapidly as shown in Fig. 5(a). The formation of cracks is proportional to thickness of hemoglobin layers of blood due to obtaining a more chance to aggregate hemoglobin together. As shown in Fig. 5(b), the ratio of white pixels to the bloodstain at high concentrations of hemoglobin showed that cracks were increasingly formed in the bloodstain. Moreover, the V values of the bloodstain decreased at highly aggregated hemoglobin because a degree of light transmission was dependent on hemoglobin concentration in Fig. 5(c).

Considering estimation of the bloodstain age at the crime scene, we applied various volume of the blood (100, 400, 700, and 1000 μL) to the comprehensive experiment under the following conditions: 23 °C temperature; 30% humidity; 15.5 g/dL hemoglobin (Fig. S6(a)). The area of the blood pool slowly decreased at 1000 μL of the blood since the moisture content increased at high blood volume, thereby drying the

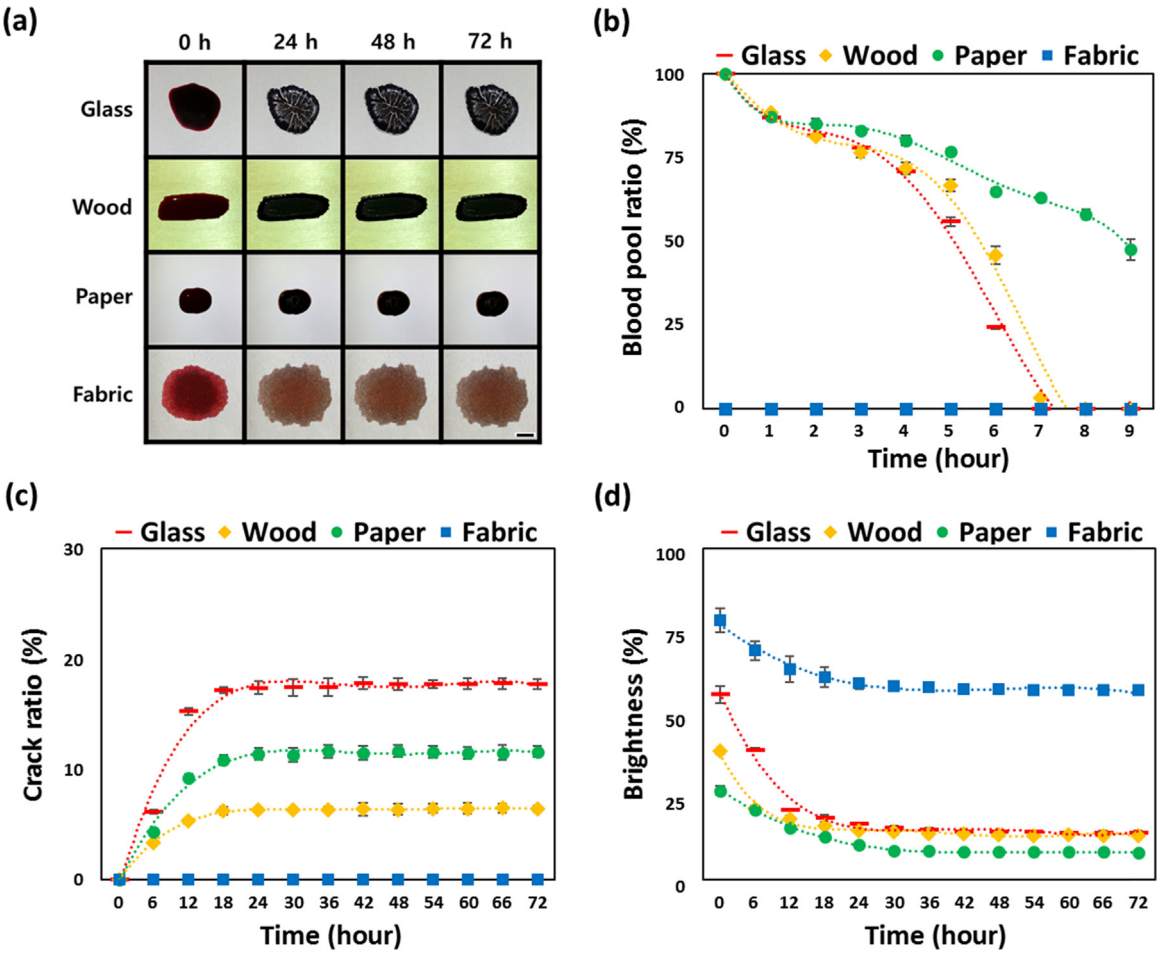

Fig. 3. (a) Four different materials (glass, wood, paper and fabric) were applied to estimate bloodstain age under the following conditions: 30% humidity, 23 °C temperature, 15.5 g/dL hemoglobin, and 700 μL sample volume (Scale bar: 1 cm). (b-d) The constant change in the blood pool area at 0–9 h, crack ratio at 0–18 h, and color intensities of bloodstains at 0–48 h were observed, respectively. (For interpretation of the references to color in this figure legend, the reader is referred to the web version of this article.).

Table 1
The degree of moisture absorption (M_i), the crack ratio, and the slopes of crack ratio for each material (glass, paper, wood, and fabric) were presented.

	Glass	Paper	Wood	Fabric
M_i (%)	0.0	11.4	48.6	100
Crack ratio (%)	17.4	11.4	6.4	0.0
Slope of crack ratio	15.3	9.3	5.4	0.0

bloodstain steadily (Fig. S6(b)). Apart from these, delaying in the drying process of the bloodstain resulted in gradual crack formation (Fig. S6(c)) and enabled to observe variation of the V values for a long time (Fig. S6(d)). However, no significant difference was observed in terms of the final results from 3 parameters (blood pool ratio, white pixel ratio, and V values) over a volume of the bloodstain ($p < 0.05$). Furthermore, no significant difference among 3 parameters was observed, whereas the whole blood dropped on 4 different materials was dried an hour earlier than the EDTA whole blood as shown in Fig. S6(a)-(d). The coefficient of variation (CV) of the variation of the bloodstain in response to various temperature and hemoglobin concentration is shown in Table S1.

4. Conclusion

In this study, we developed the smartphone-based pattern recognition system in order to enhance the accuracy and sensitivity of our previous work (Shin et al., 2017) by using three detection methods (blood pool analysis, crack ratio analysis, and colorimetric analysis) for age estimation of the bloodstain. The captured bloodstain images were successfully classified by comparing reference data of the stored images, such as blood pool ratio, white pixel ratio, and V values. We found out the obvious physical change of the blood on glass where the area of the blood pool, crack ratio over the bloodstain, and the V values were consecutively changed by 9 h, 18 h, and 48 h, respectively. Furthermore, we were able to distinguish clearly the differences in bloodstain images every hour in the early time zone by using the newly developed system. Our method possesses many advantages compared with the existing technologies for estimating postmortem interval (PMI), where rigor mortis (Bate-smith and Bendall, 1949), algor mortis (Henssge, 1988), and livor mortis (Kaatsch et al., 1993) can be replaced with the smartphone-based technologies expeditiously in terms of rapid, easy-to-use, and cost-effective methods (Shin et al., 2018). However, the bloodstain is dependent on various experimental conditions, such as temperature, humidity, and volume, so that considering such factors into our detection method is required to enhance accuracy of various conditions. In addition, we will apply such chemicals that react with bloodstains to generate color variation and deformation in order to overcome the limitation for estimating bloodstains age beyond 48 h. Thus, we envision our system to be a powerful portable tool in the forensic science fields by applying classification algorithm to enhance accuracy and sensitivity of the results.

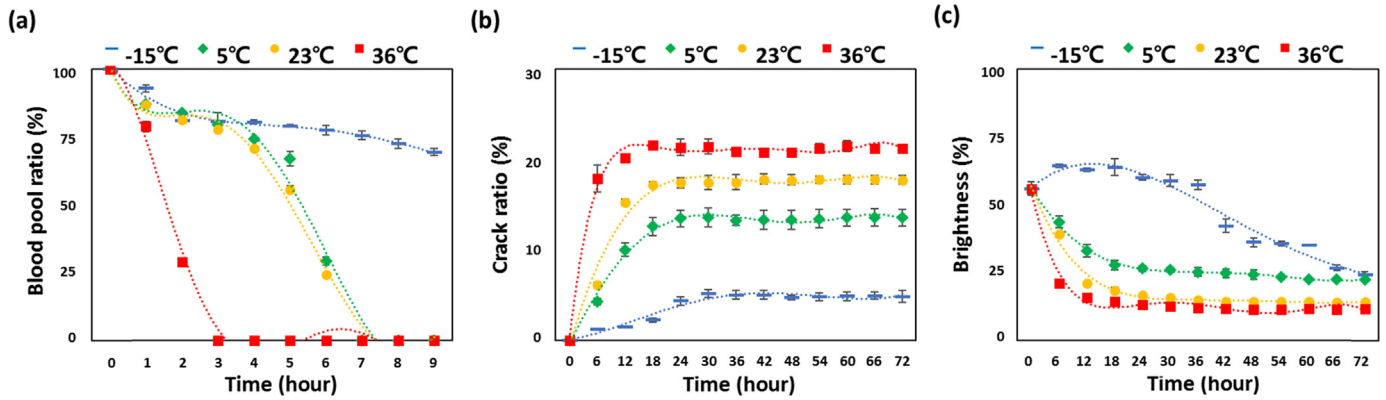

Fig. 4. The pattern change of bloodstains were monitored according to the temperature. The shrinkage of blood pool area, increment of crack formation and degradation of color intensities were observed in response to time (a: blood pool ratio, b: crack ratio, c: brightness according to temperature). Each experiment was carried out under the following condition: 30% humidity and 700 μL blood. (For interpretation of the references to color in this figure legend, the reader is referred to the web version of this article.).

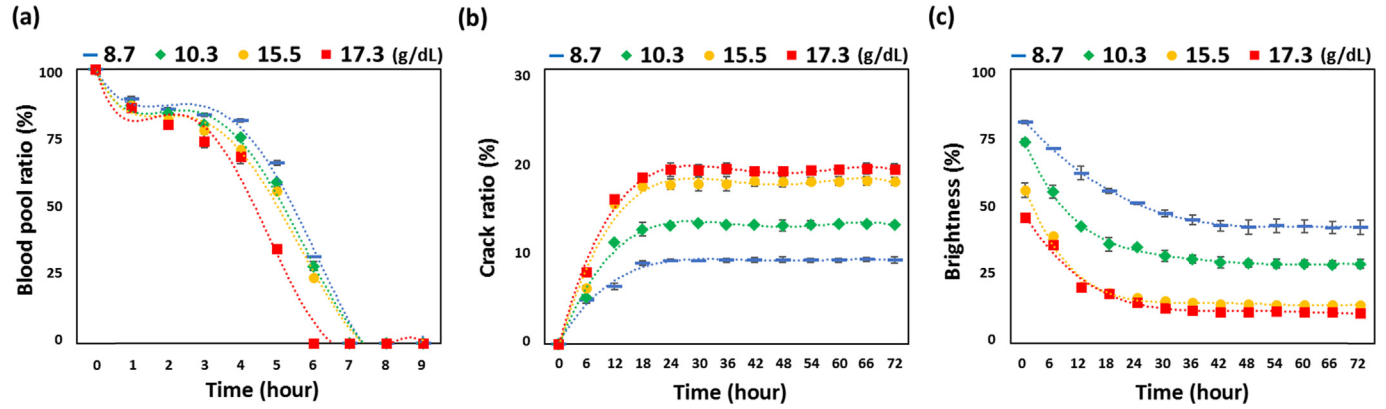

Fig. 5. The pattern change of bloodstains were monitored in response to the hemoglobin concentration. The shrinkage of blood pool area, increment of crack formation and degradation of color intensities were observed over time. (a: blood pool ratio, b: crack ratio, c: brightness in response to hemoglobin concentration). Each experiment was carried out under the following condition: 30% humidity; 23 ˚C temperature; 700 μL blood. (For interpretation of the references to color in this figure legend, the reader is referred to the web version of this article.).

Acknowledgement

This research was supported by iPET (Korea Institute of Planning and Evaluation for Technology in Food, Agriculture, Forestry and Fisheries), Ministry for Food, Agriculture, Forestry and Fisheries, Republic of Korea (316073-03-3-HD020), the Bio & Medical Technology Development Program of the NRF funded by the Korean government, MSIP (2015M3A9D7067364), and National Research Foundation of Korea (NRF) grant funded by the Korea government (MSIP) (No. 2018R1A2A2A15019814).

Appendix A. Supplementary material

Supplementary data associated with this article can be found in the online version at doi:10.1016/j.bios.2018.09.017.

References

Bate-smith, E.C., Bendall, J.R., 1949. J. Physiol. 110, 47–65.
Bauer, M., Polzin, S., Patzelt, D., 2003. Forensic Sci. Int. 138, 94–103.
Bremmer, R.H., de Bruin, D.M., de Joode, M., Buma, W.J., van Leeuwen, T.G., Aalders, M.C., 2011. PLoS One 6, e21845.
Bremmer, R.H., de Bruin, K.G., van Gemert, M.J., van Leeuwen, T.G., Aalders, M.C., 2012. Forensic Sci. Int. 216, 1–11.
Brutin, D., Sobac, B., Loquet, B., Sampol, J., 2011. J. Fluid Mech. 667, 85–95.
Chen, Y., Xu, L.P., Meng, J., Deng, S., Ma, L., Zhang, S., Zhang, X., Wang, S., 2018. Biosens. Bioelectron. 102, 418–424.
Deegan, R.D., Bakajin, O., Dupont, T.F., Huber, G., Nagel, S.R., Witten, T.A., 1997. Nature 389, 827–829.
Dugyala, V.R., Lama, H., Satapathy, D.K., Basavaraj, M.G., 2016. Sci. Rep. 6, 30708.
Furie, B., Furie, B.C., 1988. Cell 53, 505–518.
Gaertner, F., Massberg, S., 2016. Semin Immunol. 28, 561–569.
Henssge, C., 1988. Forensic Sci. Int. 38, 209–236.
Hu, H., Larson, R.G., 2002. J. Phys. Chem. 106, 1334–1344.
Hu, Z., Gu, B., Deng, A., 2012. J. Thorac. Dis. 4 (2), 235–237.
James, S.H., Kish, P.E., Sutton, T.P., 2005. Principles of Bloodstain Pattern Analysis: Theory and Practice. CRC Press, New York.
Kaatsch, H.-J., Stadler, M., Nietert, M., 1993. Int. J. Leg. Med. 106, 91–97.
Kuo, M.T., Lin, C.C., Liu, H.Y., Chang, H.C., 2011. Invest. Ophthalmol. Vis. Sci. 52 (7), 4942–4950.
Laan, N., Smith, F., Nicloux, C., Brutin, D., 2016. Forensic Sci. Int. 267, 104–109.
Lee, S., Oncescu, V., Mancuso, M., Mehta, S., Erickson, D., 2014. Lab Chip 14, 1437–1442.
Lei, H., Francis, L.F., Gerberich, W.W., Scriven, L.E., 2002. AIChE J. 48 (3), 437–451.
Shin, J., Choi, S., Yang, J.S., Song, J., Choi, J.S., Jung, H.I., 2017. Sens. Actuator B 243, 221–225.
Shin, J., Chakravarty, S., Choi, W., Lee, K., Han, D., Hwang, H., Choi, J., Jung, H.I., 2018. Analyst 143, 1515–1525.
Sobac, B., Brutin, D., 2014. Colloids Surf. A: Physicochem. Eng. Asp. 448, 34–44.
Yamanaka, E.S., Tortajada-Genaro, L.A., Pastor, N., Maquieira, A., 2018. Biosens. Bioelectron. 109, 177–183.
Yang, J.S., Shin, J., Choi, S., Jung, H.I., 2017. Sens. Actuator B 241, 80–84.
Yu, L., Shi, Z., Fang, C., Zhang, Y., Liu, Y., Li, C., 2015. Biosens. Bioelectron. 69, 307–315.